Effects of hydrophobic surface on stability and transition

Taegee Min and John Kim
Department of Mechanical and Aerospace Engineering University of California, Los Angeles, California 90095-1597

(Received 13 July 2005; accepted 27 September 2005; published online 25 October 2005)

The effects of a hydrophobic surface on stability and transition in wall-bounded shear flows are investigated. The hydrophobic surface is represented by a slip-boundary condition on the surface. The linear stability analysis with slip-boundary conditions shows that the critical Reynolds number increases with streamwise slip. The effects of slip-boundary conditions on the transient growth of initial disturbances are investigated through the singular value decomposition (SVD) analysis of the linearized Navier–Stokes equations. The maximum transient growth (i.e., the amplification factor for the optimal disturbance) is reduced with streamwise slip, indicating that non-normality of the linearized Navier–Stokes equations is reduced with streamwise slip. Finally, it is shown that the transition to turbulence is delayed significantly with streamwise slip, whereas spanwise slip induces an earlier transition. The present results suggest that it is desirable to develop a hydrophobic surface with specified directional sensitivity in order to meet a particular need for specific applications. © *2005 American Institute of Physics*. [DOI: 10.1063/1.2126569]

It has been reported that the slip velocity on hydrophobic surfaces results in a significant drag reduction in microchannel flows.[1–3] The effects of such surfaces on large-scale flows are not yet well understood. Min and Kim[4] reported that a significant drag reduction in turbulent boundary layers was unlikely with a hydrophobic surface, with the slip length on the order of a submicrometer scale that was found in nanofabricated hydrophobic surfaces. However, they reported that the amount of drag reduction achieved in their numerical experiments increased as the slip length normalized by the viscous wall units (i.e., the wall-shear velocity and kinematic viscosity) increased, thus suggesting that a significant drag reduction can be achieved in large-scale flows with a hydrophobic surface, where the slip length is on the order of several wall units. Note that for a fixed slip length, the slip length normalized by wall units increases with the Reynolds number, thus becoming more effective for high Reynolds number flows. Min and Kim[4] also reported that the skin-friction drag was reduced with streamwise slip, while spanwise slip showed the opposite effect. A surface with combined slip, which would be the case for most hydrophobic surfaces currently available, resulted in a smaller net reduction than streamwise-only slip surfaces.

The effects of hydrophobic surfaces on flow stability and the transition to turbulence are of great interest for many engineering applications. The delay of transition in microchannels, for example, can lead to a substantial reduction in the power required to move the fluid inside. The potential benefit that can be achieved from the delay of transition in larger-scale flows are enormous. Our objective in this study was to extend our previous findings,[4] by investigating the effects of the hydrophobic surface on stability (linear effect) and transition (nonlinear effect). A linear stability analysis with slip boundary conditions was performed, to characterize the stability associated with hydrophobic surfaces, and numerical experiments were performed to investigate the effects on the transition to turbulence. In addition, the singular value decomposition (SVD) analysis of the linearized Navier–Stokes equations, which provided useful insights into the control of turbulent boundary layers,[5] was carried out to elucidate the effects of slip velocity on stability and transition.

In this paper, we shall use u, v, and w to denote, respectively, the velocity component in the streamwise (x), wall–normal (y), and spanwise (w) directions. All quantities are normalized by the laminar centerline velocity, U_c (1.5 times greater than the bulk mean velocity), the channel half-width, δ, and the kinematic viscosity, ν, unless stated otherwise.

Experimental studies[1,2] have shown that flows with a hydrophobic surface can be analyzed by the Navier–Stokes equations with a slip-boundary condition:

$$u_s = L_s \left.\frac{\partial u}{\partial y}\right|_{\text{wall}}, \quad w_s = L_s \left.\frac{\partial w}{\partial y}\right|_{\text{wall}}, \tag{1}$$

where u_s and w_s denote the streamwise and spanwise slip velocity, respectively, and L_s denotes the slip length.

By substituting the wall–normal velocity perturbation in the normal-mode form, $v(x,y,t)=\hat{v}(y)\exp[i\alpha(x-ct)]$ into the linearized Navier–Stokes equations for two-dimensional channel flows, we obtain the following Orr–Sommerfeld (OS) equation:

$$[(U-c)\Delta - D^2U - (i\alpha\,\mathrm{Re})^{-1}\Delta^2]\hat{v} = 0, \tag{2}$$

where α and c denote, respectively, the streamwise wave number and the wave speed, D represents the derivative with respect to y, $\Delta = D^2 - \alpha^2$, U is the mean velocity, $\mathrm{Re} = U_c\delta/\nu$ the Reynolds number, and the overcaret denotes a Fourier-transformed quantity. The relevant mean velocity and slip-boundary conditions are

$$U = \frac{2L_s + 1 - y^2}{3L_s + 1}, \quad \hat{v}(\pm 1) = 0, \quad D\hat{v}(\pm 1) = \mp L_s D^2 \hat{v}(\pm 1). \tag{3}$$

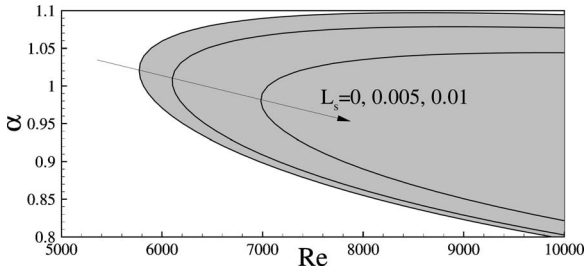

FIG. 1. Neutral curve with slip length.

Note that U satisfies the slip-boundary condition given in Eq. (1), and it has the same mass flux as that of the plane Poiseuille flow with no slip ($U=1-y^2$). The boundary conditions for $D\hat{v}$ and $D^2\hat{v}$ are direct consequences of the continuity equation $i\alpha\hat{u}+D\hat{v}=0$.

Temporal stability problems (i.e., finding complex c for a given real α) were considered in the present study. A Chebyshev-tau method was used to solve Eqs. (2) and (3). The results are shown in Fig. 1, where the neutral stability curves for different slip lengths are plotted. The shaded region represents the linearly unstable region, where the imaginary part of the eigenvalue $\omega=\alpha c$ in Eq. (2) is positive. It is apparent that the slip-boundary condition makes the flow more stable, and that the critical Reynolds number (Re_{cr}) increases with the slip length, while the range of streamwise wave numbers corresponding to the unstable region decreases. These results are in agreement with those of Gersting[6] and Spille *et al.*[7] Contrary to these findings, Chu[8] recently reported that a slip-boundary condition decreased, Re_{cr} drastically. The mean velocity and the boundary conditions considered by Chu were

$$U = 1 - y^2 + 2L_s, \quad \hat{v}(\pm 1) = 0, \quad D\hat{v}(\pm 1) = 0. \tag{4}$$

Note that only the mean velocity was modified to account for the slip boundary condition given in Eq. (1), and a no-slip boundary condition was used for $\hat{v}$. The use of no-slip boundary conditions for perturbations on a hydrophobic surface is obviously incorrect. For such a surface, however, it can be easily shown that the solution to Eqs. (2) and (4) is simply

$$v = \hat{v}(y)\exp\{\mathrm{i}\alpha[x - (c + 2L_s)t]\}, \tag{5}$$

where $\hat{v}$ is the solution for a regular channel (i.e., $U=1-y^2$ with a no-slip boundary condition for $\hat{v}$). Thus, if ω is an eigenvalue for a regular channel, eigenvalues for the system considered by Chu[8] are

$$\omega^* = \omega + 2\alpha L_s. \tag{6}$$

Since we are presently considering temporal stability, for which α is real and the imaginary part of the eigenvalues determines the stability, the neutral stability curve for the system considered by Chu must be the same as that for a regular channel ($L_s=0$).

The eigenvalue analysis given above, which predicts whether a small (linear) disturbance can grow or decay asymptotically, is inadequate in explaining transient growth of the kinetic energy of certain disturbances in an otherwise

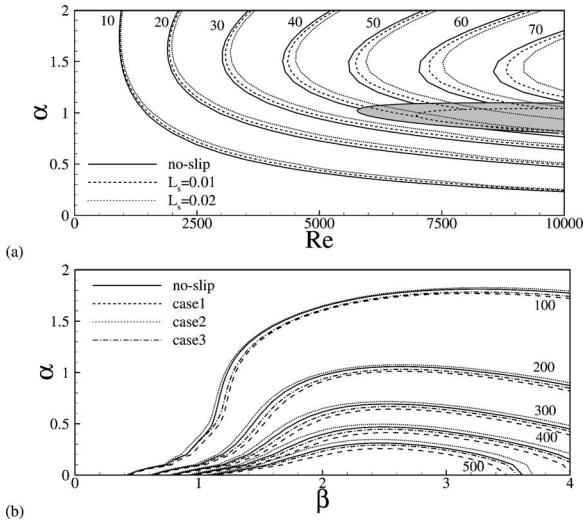

FIG. 2. Contours of $G_{\max}$: (a) $\alpha\neq 0$ and $\beta=0$; (b) $\alpha\neq 0$, $\beta\neq 0$, Re=2000, and $L_s=0.01$.

stable system. It has been shown that transient growth can be analyzed by applying the singular value decomposition (SVD) analysis to the linearized Navier–Stokes equations.[5] We applied the same approach used by Lim and Kim[5] (see also Refs. 9 and 10) to the linearized Navier–Stokes equations with the modified mean velocity as given in Eq. (3). Here, we present a brief overview of the SVD analysis for completeness, but the interested reader is referred to Lim and Kim[5] for further details.

The linearized Navier–Stokes equations can be written in terms of v and wall–normal vorticity ω_y as

$$\frac{\partial}{\partial t}\begin{bmatrix} v \\ \omega_y \end{bmatrix} = [\mathcal{A}]\begin{bmatrix} v \\ \omega_y \end{bmatrix}, \tag{7}$$

where

$$[\mathcal{A}] = \begin{bmatrix} \Delta^{-1}\left(-U\frac{\partial}{\partial x}\Delta + D^2U\frac{\partial}{\partial x} + \frac{1}{\mathrm{Re}}\Delta^2\right) & 0 \\ -DU\frac{\partial}{\partial z} & -U\frac{\partial}{\partial x} + \frac{1}{\mathrm{Re}}\Delta \end{bmatrix}. \tag{8}$$

Here, $\Delta=D^2-\alpha^2-\beta^2$, α and β denote the streamwise and spanwise wave number, respectively. The linear operator $\mathcal{A}$ is non-normal (i.e., not self-adjoint), and hence, its eigenmodes are nonorthogonal to each other, which allows transient growth of kinetic energy, even if all individual eigenmodes are stable and decay asymptotically. To analyze the optimal transient energy growth, we consider the ratio of

TABLE I. $G_{\max}$ for wave number pairs (α,β) at Re=2000 and $L_s=0.01$.

(α,β)	No slip	Case 1	Case 2	Case 3
(0,2)	783.2	746.3	821.0	782.6
(0.5,1)	80.50	76.01	84.38	79.60
(1,3)	207.7	198.6	211.9	202.4
(2,4)	121.4	116.8	123.4	118.7

TABLE II. Variation of the largest $G_{\max}$ with Re and L_s.

	No slip	$L_s=0.005$			$L_s=0.01$			$L_s=0.02$		
Re		Case 1	Case 2	Case 3	Case 1	Case 2	Case 3	Case 1	Case 2	Case 3
1000	196.2	191.5	200.9	196.1	186.9	205.5	195.9	178.3	214.4	195.2
2000	783.8	764.9	802.7	783.5	746.7	821.2	782.8	712.1	856.6	779.9
5000	4897	4779	5015	4895	4665	5131	4891	4448	5352	4873

kinetic energy of a disturbance at a given time τ to that at $t=0$,

$$G(\tau)=\sup_{\mathbf{x}(0)\neq 0}\frac{||\mathbf{x}(\tau)||_e}{||\mathbf{x}(0)||_e}, \tag{9}$$

where the energy norm

$$||\mathbf{x}||_e^2\equiv\int_{-1}^{1}\left[\hat{v}^*\hat{v}+\frac{1}{\alpha^2+\beta^2}\left(\frac{\partial\hat{v}^*}{\partial y}\frac{\partial\hat{v}}{\partial y}+\hat{\omega}^*\hat{\omega}\right)\right]dy, \tag{10}$$

represents kinetic energy. The energy norm can be expressed as

$$\begin{aligned}||\mathbf{x}(\tau)||_e^2&=\mathbf{x}^*(\tau)\mathbf{F}^*\mathbf{F}\mathbf{x}(\tau)=||\mathbf{F}\mathbf{x}(\tau)||_2^2\\&=||\mathbf{F}\exp(\mathbf{A}\tau)\mathbf{x}(0)||_2^2,\end{aligned} \tag{11}$$

where $||\cdot||_2$ represents the 2-norm (Euclidian norm). Substituting Eq. (11) into Eq. (9), we obtain

$$\begin{aligned}G(\tau)&=\sup_{\mathbf{x}(0)\neq 0}\frac{||\mathbf{F}\exp(\mathbf{A}\tau)\mathbf{x}(0)||_2^2}{||\mathbf{F}\mathbf{x}(0)||_2^2}\\&=\sup_{\mathbf{w}(0)\neq 0}\frac{||\mathbf{F}\exp(\mathbf{A}\tau)\mathbf{F}^{-1}\mathbf{w}(0)||_2^2}{||\mathbf{w}(0)||_2^2}.\end{aligned} \tag{12}$$

Equation (12) is the definition of the 2-norm of matrix $\mathbf{F}\exp(\mathbf{A}\tau)\mathbf{F}^{-1}$, and it corresponds to the largest singular value of the matrix.

For each wave number pair of α and β, the largest $G(\tau), G_{\max}$ was computed, and the results are shown in Fig. 2. In order to delineate the effect of streamwise and spanwise slips, separately, three different cases were considered: (1) case 1, streamwise slip ($u_s\neq 0$, $w_s=0$); (2) case 2, spanwise slip ($u_s=0$, $w_s\neq 0$); and (3) case 3, combined slip ($u_s\neq 0$, $w_s\neq 0$). The effect of streamwise slip is shown in Fig. 2(a), where $G_{\max}$ for $\alpha\neq 0$ and $\beta=0$ (i.e., two-dimensional disturbances) is shown as a function of α and Re. It is apparent that for a given Reynolds number and wave number, $G_{\max}$ is reduced proportionally to the slip length. Note that $G_{\max}$ is infinity for unstable eigenmodes, and the shaded region in Fig. 2(a) represents this unstable region. In order to investigate the effect of spanwise slip, $G_{\max}$ was computed as a function of α and β for Re=2000 and $L_s=0.01$, and the results are shown in Fig. 2(b) and summarized in Table I. For a given α and β, the streamwise slip reduces $G_{\max}$, whereas the spanwise slip enhances $G_{\max}$. For the combined slip (case 3), there is a slight net reduction.

Trefethen *et al.*[11] reported that the largest $G_{\max}$ for the no-slip boundary condition was obtained at $\alpha=0$ and $\beta\simeq 2$, and the maximum value was proportional to $\mathcal{O}(\mathrm{Re}^2)$. The largest $G_{\max}$ for the slip boundary condition was also obtained at $\alpha=0$ and $\beta\simeq 2$. The largest $G_{\max}$ for different Re and L_s is given in Table II. The largest $G_{\max}$ was also proportional to $\mathcal{O}(\mathrm{Re}^2)$ with the slip-boundary condition, and the increase/decrease was proportional to L_s.

The eigenvalue analysis as well as the SVD analysis presented are linear analyses, and they do not provide definite information on the transition to turbulence, since nonlinear effects must be accounted for. The effect of hydrophobic surfaces on transition was investigated through direct numerical simulations of a channel flow with slip boundary conditions. Temporal transition, similar to that studied by Sandham and Kleiser,[12] was investigated in the present work. A pseudospectral code similar to that used by Kim *et al.*,[13] was used for the present study. Simulations were conducted at $\mathrm{Re}=U_c\delta/\nu=5000$, and the computational domain of $(2\pi/\alpha_0)\delta\times 2\delta\times(2\pi/\beta_0)\delta$ was used in the streamwise, wall–normal, and spanwise directions, respectively, with $128\times 129\times 128$ grids. Here, α_0(=1.12) and β_0(=2.1) were the fundamental wave numbers in the streamwise and spanwise directions, respectively. In order to simulate the ribbon-induced transition, all calculations were started with a finite-amplitude (amplitude 3%) Tollmien–Schlichting (TS) wave,

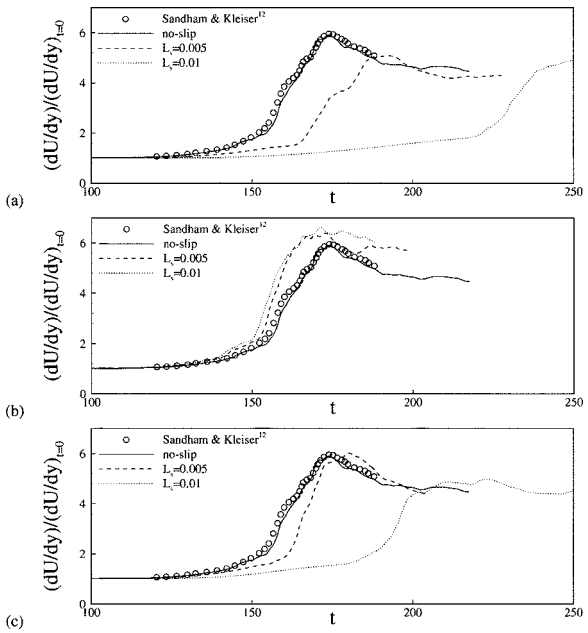

FIG. 3. Time histories of mean velocity gradients normalized by the laminar value: (a) case 1; (b) case 2; (b) case 3.

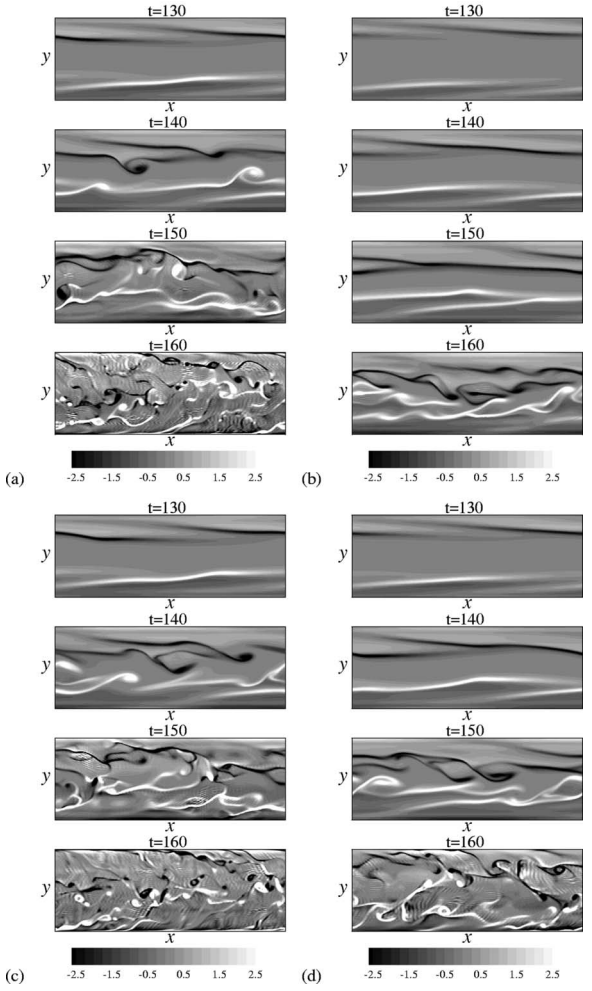

FIG. 4. Spanwise vorticity (ω_z) in the x-y plane at $z=\pi/\beta_0$ for $L_s=0.005$: (a) no slip; (b) case 1; (c) case 2; (d) case 3.

together with two equal and opposite oblique waves of amplitude 0.1% (for details, see Sandham and Kleiser[12]).

A constant mass flow rate was maintained for all cases, and the computations were carried out until the mean velocity gradient at the wall, $(dU/dy|_w)$ reached a fully turbulent state after transition. Figure 3 shows time histories of $dU/dy|_w$ normalized by the laminar value $(2/3L_s+1)$. The streamwise slip (case 1) delayed transition significantly, whereas spanwise slip (case 2) induced an earlier transition. For combined slip (case 3), the transition delay was less pronounced due to the adverse effect of spanwise slip. It is apparent that the slip effect on transition was proportional to the slip length for all cases. It is quite remarkable that a very small amount of slip (0.01δ) yields such a pronounced impact on transition (on the order of 50δ, using the centerline velocity as the convection velocity to convert the time delay into spatial delay). The slip effect on transition seems to be quite large, considering relatively small changes in $G_{\max}$ shown above. Recall that the SVD analysis, from which $G_{\max}$ was computed, is a linear analysis, in which the mean velocity is fixed. The transition simulations include nonlinear effects, which modify the mean velocity used in the SVD analysis. It appears that this nonlinear effect strengthens the slip effect on transition. It is also worth noting that the slip effect on transition is consistent with the slip effect on skin-friction drag in turbulence channel flow, where the drag was decreased/increased by streamwise/spanwise slip proportionally to the slip length.[4]

Figure 4 shows contours of spanwise vorticity (ω_z) in the x-y plane at $z=\pi/\beta_0$ for $L_s=0.005$. A typical sequence of transition in regular channel flow is also shown in Fig. 4(a) for a comparison. A high-shear layer rolls into spanwise vortices at $130<t<140$, followed by the eventual breakdown at $150<t<160$ (for a comparison and further details of transition in a regular channel, see Sandham and Kleiser[12]). The delay of transition by streamwise slip is apparent in Fig. 4(b), whereas the roll-up and breakdown take place a bit earlier than the regular channel with spanwise slip [Fig. 4(c)]. For combined slip [Fig. 4(d)], transition takes place earlier than that with streamwise slip, but much later than that of a regular channel.

We have shown that the slip boundary condition on a hydrophobic surface has a significant impact on stability and transition. Streamwise slip increases the critical Reynolds number with the increase proportional to the slip length. The transient growth is decreased/increased with streamwise/spanwise slip, thus indicating that non-normality of the linear operator is reduced/increased with streamwise/spanwise slip. The transition to turbulence is delayed with streamwise slip, while the opposite is observed with spanwise slip.

This work has been supported by the Air Force Office of Scientific Research (F49620-03-1-0038, Dr. Beutner; F49620-03-1-0244, Dr. Heise). The computer time provided by the National Science Foundation (NSF) through TeraGrid resources is gratefully acknowledged.

[1] D. C. Tretheway and C. D. Meinhart, "Apparent fluid slip at hydrophobic microchannel walls," Phys. Fluids **14**, L9 (2002).
[2] C. Choi, K. J. A. Westin, and K. S. Breuer, "Apparent slip flows in hydrophilic and hydrophobic microchannels," Phys. Fluids **15**, 2897 (2003).
[3] J. Kim and C. J. Kim, "Nanostructured surfaces for dramatic drag reduction of flow resistance in droplet-based microfluidics," Technical Digest, *IEEE Conference on MEMS*, Las Vegas, NV, 2002, p. 479.
[4] T. Min and J. Kim, "Effects of hydrophobic surface on skin-friction drag," Phys. Fluids **16**, L55 (2004).
[5] J. Lim and J. Kim, "A singular value analysis of boundary layer control," Phys. Fluids **16**, 1980 (2004).
[6] J. M. Gersting, "Hydrophobic stability of plane porous slip flow," Phys. Fluids **17**, 2126 (1974).
[7] A. Spille, A. Rauh, and H. Bühring, "Critical curves of plane Poiseuille flow with slip boundary conditions," Nonlinear Phenom. Complex Syst. (Dordrecht, Neth.) **3**, 171 (2000).
[8] A. K-H, Chu, "Instability of Navier slip flow of liquids," C. R. Mec. **332**, 895 (2004).
[9] S. C. Reddy and D. S. Henningson, "Energy growth in viscous channel flows," J. Fluid Mech. **252**, 209 (1993).
[10] P. J. Schmid and D. S. Henningson, *Stability and Transition in Shear Flows* (Springer, New York, 2001).
[11] L. N. Trefethen, A. E. Trefethen, S. C. Reddy, and T. A. Driscoll, "Hydrodynamic stability without eigenvalues," Science **261**, 578 (2004).
[12] N. D. Sandham and L. Kleiser, "The late stages of transition to turbulence in channel flow," J. Fluid Mech. **245**, 319 (1992).
[13] J. Kim, P. Moin, and R. Moser, "Turbulence statistics in fully developed channel flow at low Reynolds number," J. Fluid Mech. **177**, 133 (1987).